Sunglint removal in high spatial resolution hyperspectral images under different viewing geometries

Annia Susin Streher[1]
James A. Goodman[2]
Lênio Soares Galvão[1]
Claudio Clemente Faria Barbosa[1]
Thiago Sanna Freire Silva[1]
Evlyn Marcia Leão de Moraes Novo[1]

[1] Instituto Nacional de Pesquisas Espaciais -INPE
Caixa Postal 515 - 12227-010 - São José dos Campos - SP, Brazil
{annia, claudio}@dpi.inpe.br; {lenio, thiago, evlyn}@dsr.inpe.br

[2] HySpeed Computing
PO Box 431824, Miami, FL 33243 USA
{jgoodman}@hyspeedcomputing.com

Abstract. Sunglint, also known as specular reflection of light from water surfaces into sensor optics, is a component of sensor-incoming radiance that represents a degrading factor on the spectral characterization of water bodies. Airborne remote sensors are suitable to evaluate and monitor freshwater ecosystems, unfortunately those sensors can be heavily affected by sunglint, due to their high spatial resolution. Although, sunglint effects can be minimized in airborne remote sensing by optimizing the viewing geometry, those conditions cannot always be applied, due to the size and spatial pattern of inland water bodies, so methods to identify and correct for extraneous radiance contributions are essential. The present study reviews current techniques to remove sunglint radiance component from high spatial resolution images and tests a deglint algorithm in a set of airborne hyperspectral images acquired under different viewing geometry. The results demonstrate the sunglint effects damaging the images, directly influencing its visual aspects, the magnitude of the image spectra under glint conditions and masking the correlations between the optically active substances and the spectral data. The algorithm applied showed good results removing the sunglint in the images, providing a viable solution to mitigate those effects in higher resolution hyperspectral images of optically complex waters, acquired by airborne sensors.

Keywords: airborne remote sensing, water surface specular reflection, case II waters, optically active substances.

1. Introduction

Airborne remote sensing, given its versatility, has certain advantages over spaceborne sensors for monitoring inland, estuarine and coastal waters. For instance, the spatial extent of inland water bodies is generally smaller than the resolving power of satellite sensors, making it difficult to retrieve pure water pixels from images acquired over most freshwater ecosystems. On the other hand, airborne sensors can have variable, much finer spatial resolution when compared to that of most spaceborne sensors. Additionally, the few high spatial resolution satellite sensors currently available (*e.g.* Ikonos, Quickbird and WorldView), lack the spectral resolution and sensitivity to detect and estimate chlorophyll-a concentration in optically complex waters (Kutser et al. 2006, Moses et al., 2012). Another advantage of most airborne sensors is that the number; location and bandwidths of spectral channels are adjustable (Bertels et al., 2008; Moses et al., 2012), making them suitable for evaluating and distinguishing photosynthesizing pigments, a key component for case II waters characterization.

Airborne remote sensors, however, can be heavily affected by sunglint. The sunglint effect happens when the water surface orientation is such that the sun light is directly reflected towards the sensor and is a function of the water surface roughness, sun position and viewing geometry (Kay et al., 2009). Sunglint adds a radiation component to the signal registered by the sensor

which does not carry any information about the water column, and is typically much higher than the water leaving signal in all spectral bands. This effect can saturate pixel values and obscure the information on chlorophyll concentration and other optically active substances (OAS), requiring higher radiometric sensitivities to properly register useful information.

In airborne remote sensing data, the effect of sunglint can be minimized by optimizing the flight paths, directing the sensor towards or away from the Sun (Mustard et al., 2001), and by keeping solar zenith angles between 30° and 60° (Dekker et al., 2001). However, those guidelines cannot always be applied, often due to the size and spatial pattern of water bodies. The sinuous and irregular forms of meandering rivers and man-made lakes are a major challenge in planning image acquisition using sensors with a narrow field of view, since different acquisition geometries are needed to cover the entire area. In such cases, sunglint effects may become a serious damaging factor for accurately determining the optical characteristics of water bodies from remotely sensed data, requiring specific methods for reducing its effects on the acquired images.

1.1 Methods of sunglint removal

Most sunglint removal algorithms for high resolution images use the near infrared (NIR) band for estimating the amount of sunglint in each pixel (Kay et al., 2009, Casal et al., 2011). These algorithms assume that the water leaving signal is negligible in this spectral region, and that any remaining signal after atmospheric correction is caused by sunglint. Under this assumption, the spectrum from deeper regions of the water body (with high absorption in the NIR range) is used to define a linear relationship between the NIR infrared reflectance and sunglint reflectance (Hochberg et al., 2003; Hedley et al., 2005; Lyzenga et al., 2006). The linear relationship between visible (VIS) and NIR glint radiances has its physical basis on the water refraction index, which is (nearly) the same at VIS and NIR wavelengths (Mobley, 1994). However, it is important to point out that it is not always possible to assume that NIR reflectance from inland water bodies is negligible, as it may be affected by bottom reflectance, inorganic particle concentration, and phytoplankton scattering. For example, the methods developed by Hochberg et al. (2003) and Hedley et al. (2005) overcorrect the sunglint signal in shallow water imagery (*e.g.* in waters less than about 2 m deep or with high mineral turbidity) (Goodman et al., 2008; Kutser et al., 2009). Another weakness of those methods, according to Kay et al. (2009), is the assumption that the relationship between VIS and NIR wavelengths observed for deep water regions will hold for the entire image, which may not be true if atmospheric properties are not uniform. Furthermore, these methods were developed for multispectral images, and are not readily adaptable to operational use in hyperspectral data.

Alternative methods are suggested by Goodman et al. (2008) and Kutser et al. (2009), which developed sunglint algorithms for hyperspectral images. Kutser et al. (2009) algorithm is based on the 763 nm oxygen absorption band; if atmosphere correction is effective, then reflectance in this band should be zero, and any remaining signal can be attributed to sunglint effects. Despite the good results shown by the authors, the method is too sensitive to atmospheric correction procedures, which may generate spurious signals and prevent its application. The method developed by Goodman et al. (2008) is based on Lee et al. (1999) model, and assumes that reflectance at 750 nm should approach zero, except in cases it may be larger than zero (*e.g.* shallow areas in clear water). The algorithm thus allows for values at 750nm to be greater than zero, according to the signal observed at 640nm. In addition, the correction coefficients used by the method are sensor-independent, and therefore equally applicable to any dataset. Lee et al. (2012) have successfully applied the Goodman et al. (2008) method for sunglint removal in WorldView-2 multispectral imagery, while attempting to retrieve ocean depth in Hawaii. The method also allows for sunglint correction under situations of cross-scene variation, as each pixel is corrected independently (Kay et al., 2009), but it applies the same correction for each

wavelength, assuming that sunglint is spectrally flat. Kay et al. (2009) suggests that an improvement to the method would be to introduce a wavelength dependent sunglint correction.

Given the above, the present study evaluates the effectiveness of the sunglint removal procedure proposed by Goodman et al. (2008) to correct sunglint effects in airborne hyperspectral high resolution images, and assesses its effectiveness in improving the spectral characterization of optically active substances in case II waters, for an inland freshwater reservoir in São Paulo, Brazil.

2. Methods

Ibitinga reservoir is located in the central region of the state of São Paulo (Brazil), within the Tietê River basin (Figure 1). The reservoir has a meandering shape, demanding constant changes in acquisition geometry to achieve complete coverage, therefore not allowing sunglint conditions to be minimized during image acquisition.

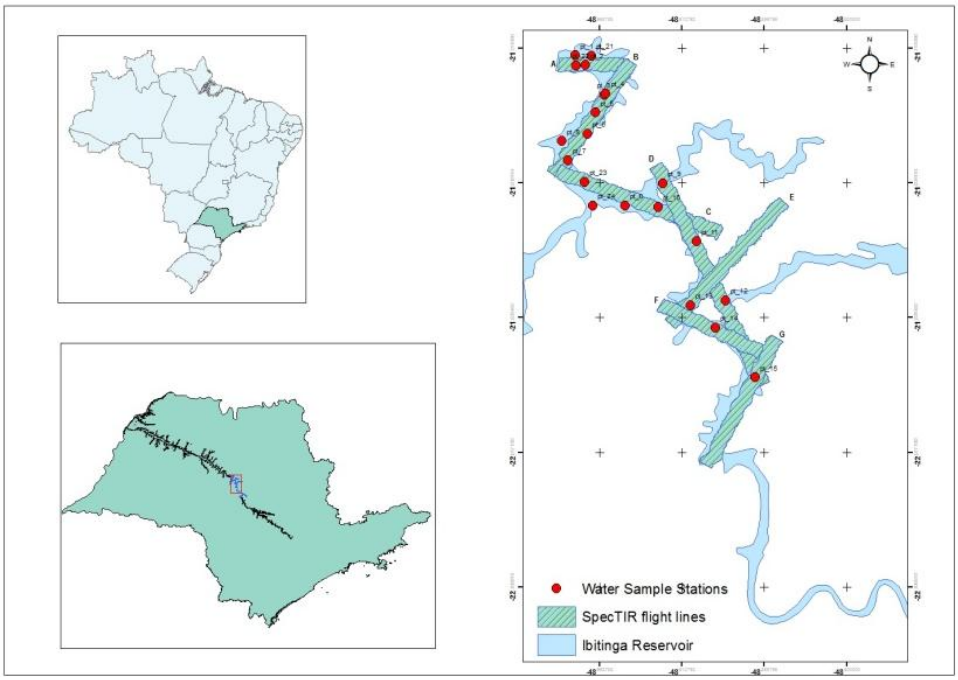


Figure 1. Location of Ibitinga reservoir, in the state of São Paulo, Brazil. Multiple airborne hyperspectral images have been acquired for the study of water optical properties. Image footprints and field sampling stations are shown in red and green, respectively, on the right.

Field data collection was carried out on October 23rd and 24th, 2011. During these two days, 19 stations along the reservoir were sampled and on the second day, the sampling occurred concurrently with the image acquisition using the SpecTIR sensor, operated by the FotoTerra company.

Chlorophyll-a (chla) was extracted from samples using 80% ethanol at a temperature of 75ºC, left to cool in the dark for 6 to 24h, and then quantified by spectrophotometer analysis (Nusch, 1980). After chlorophyll quantification, the same sample was acidified with HCl 0,4N to assess pheophytin concentration (feof). The concentrations of inorganic suspended solids (SS_inor), organic suspended solids (SS_org), and total suspended solids (TSS) were determined according to Wetzel and Likens (1991), and total dissolved carbon and organic dissolved carbon concentrations were determined by a TOC analyzer. Supplementary *in situ* measurements included Secchi disk depth.

The SpecTIR airborne sensor operates in the visible/near-infrared (VNIR) wavelengths between 400 and 1000 nm, and short-wave infrared (SWIR) wavelengths between 1000 and 2500 nm. This sensor has already been successfully applied to estimate different chlorophyll-a

concentrations in water bodies (Ferreira et al., 2011) and in land remote sensing studies (Pontius et al. 2008; Naumann et al. 2009). The variable acquisition geometry observed for this mission allowed the assessment of sunglint effects over different illumination and viewing angles (Table 1). All scenes were acquired at nadir, with a pixel size of 3m x 3m.

Table 1. SpecTIR sensor image acquisition features over the Ibitinga Reservoir (São Paulo, Brazil).

Code	**Starting latitude and longitude**		**Ending latitude and longitude**		**Local time**		**Sun Zenith angle (º)**	**Sun Azimuth angle (º)**	**Average flight height (km)**
	S	*W*	*S*	*W*	*Initial*	*Final*			
A	21°45'40.92"	48°59'49.13"	21°45'43.09"	48°57'1.61"	09:23:52	09:24:52	52.7	88.3	2.748
B	21°50'5.32"	48°59'59.04"	21°45'32.39"	48°56'50.44"	09:33:20	09:35:29	50.4	87.2	2.741
C	21°49'54.67"	48°59'52.39"	21°52'19.84"	48°53'16.24"	10:27:54	10:30:28	37.9	80.7	2.748
D	21°49'45.31"	48°55'47.96"	21°58'22.09"	48°51'28.89"	10:37:08	10:40:39	35.6	79.4	2.747
E	21°55'56.98"	48°55'13.14"	21°51'8.04"	48°50'38.77"	10:18:30	10:20:52	39.9	82.0	2.753
F	21°55'10.78"	48°55'38.73"	21°57'10.09"	48°51'20.91"	10:45:51	10:47:36	33.7	77.9	2.755
G	22°1'32.00"	48°53'44.36"	21°56'31.70"	48°50'54.29"	10:54:02	10:56:02	31.7	76.3	2.760

Atmospheric correction was performed using the Fast Line-of-sight Atmospheric Analysis of Spectral Hypercubes (FLAASH) algorithm, as implemented in the ENVI 4.8 software. Each scene was individually corrected, using specific features such as central pixel latitude and longitude, date and time of image acquisition, flight height, pixel size, and ground surface altitude. These parameters were provided by FotoTerra. All images were corrected using the Tropical Atmosphere model, and the Rural particle model for aerosol type. Water vapor content was determined using the 1135 nm SpecTIR band, and visibility (atmospheric extinction coefficient) was set to larger than 70 km for all scenes. After atmospheric correction, pixel values were scaled to surface reflectance, making it possible to spectrally characterize the different water masses. Geometric correction was then performed on each atmospherically correct reflectance image using the Map Tools package in ENVI 4.8. The Geometry Look-up Table (GLT) input data used for geometric correction was also provided by FotoTerra.

To simplify the spectral analyses of water masses, a water surface mask was generated to exclude all non open-water pixels in the images. The masks were drawn manually using the ROI tool available in ENVI 4.8. All land, macrophyte stands, boats, clouds and cloud shadows were removed, leaving strictly open-water pixels.

2.1 Sunglint removal algorithm

The Goodman et al. (2008) algorithm was selected due to its simplicity, low computational cost and evidence of success based on current literature (Goodman et al., 2008; Kay et al., 2009, Lee et al., 2012). The algorithm takes above water remote sensing reflectance R_{rs}^{raw} (sr^{-1}) as input, which was approximated by multiplying the surface reflectance values by π. The sunglint correction is calculated as a constant offset across all wavelengths, depending on the difference between R_{rs} at 640 and 750 nm, according to the following equations (Equations 1 and 2):

$$R_{rs}(\lambda) = R_{rs}^{raw}(\lambda) - R_{rs}^{raw}(750) + \Delta \quad (1)$$

$$\Delta = 0{,}000019 + 0{,}1[R_{rs}^{raw}(640) - R_{rs}^{raw}(750)] \quad (2)$$

where $R_{rs}(\lambda)$ is the deglinted remote sensing reflectance at all wavelengths; $R_{rs}^{raw}(\lambda)$ is the above water remote sensing reflectance at all wavelengths; $R_{rs}^{raw}(750)$ is the above water remote

sensing reflectance at 750 nm; $R_{rs}^{raw}(640)$ is the above water remote sensing reflectance at 640 nm, and Δ is the offset added to each wavelength. The constants 0,000019 and 0,1 were provided by Lee et al. (1999) and, according to the authors, can be applied to images obtained by any hyperspectral sensor, as long as there are bands located at 750nm and 640nm.

After sunglint correction, the resulting images were converted back to surface reflectance to allow for easier interpretation of the results.

3. Results and Discussion

Visual inspection of the sunglint-free products shows that the deglint algorithm improves the radiometric quality of the images, removing the visual effects of the cross-track and wave-induced sunglint (Figure 2).

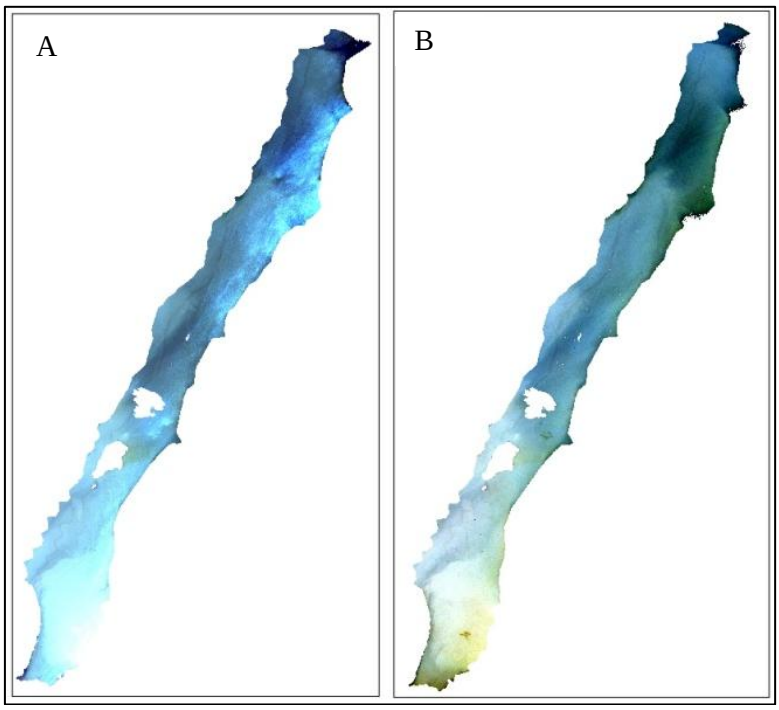


Figure 2. True color composition (R: 638nm G: 548nm B: 460nm) using SpecTIR images of Ibitinga reservoir. A) image affected by sunglint, B) image after sunglint removal. Notice the change in water color, likely caused by pigments, on the top portion of the image, as well as increased detail observable for the sediment plume located at the bottom of the scene.

An important aspect provided by the method was the ability to preserve the spectral relationships after sunglint removal. This result can be shown by analyzing the overlapping region between two different flight tracks. These areas should have similar reflectance spectra, as they represent the same target imaged under different geometries. As shown in Figure 3, the spectra under sunglint conditions have different magnitudes, but match very closely after the application of the Goodman et al. (2008) algorithm. Another important consideration is that the algorithm does not change the shape of the spectra, thereby preserving the spectral features of the target. Otherwise, if either the shape or magnitude of the reflectance spectra is modified, then results from further analysis may be dubious. For example, reflectance spectra of algal blooms and seagrass beds are similar in shape but different in magnitude (Vahtmäe et al., 2006); therefore, both features must be considered for evaluation and characterization of water bodies.

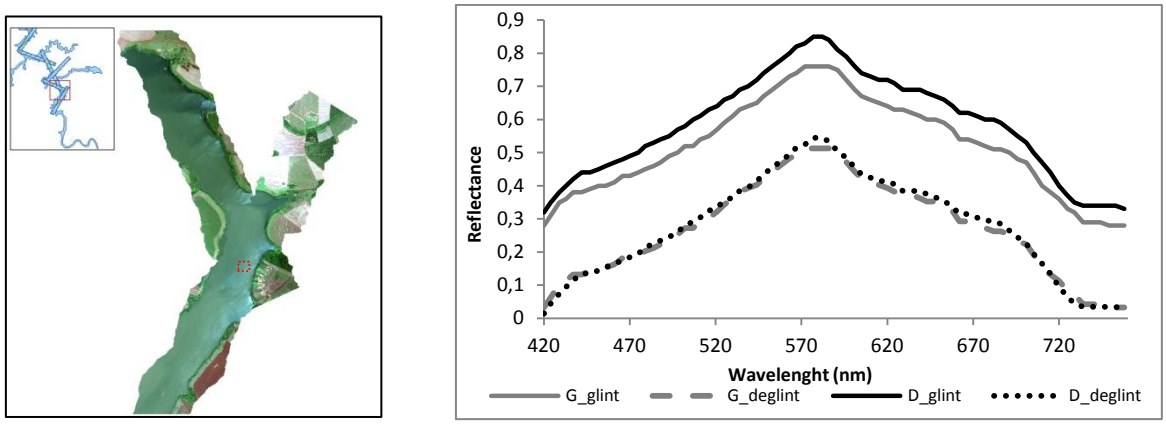


Figure 3. Reflectance spectra of a sample with pixels from two overlapping SpecTIR airborne images of Ibitinga reservoir, before and after sunglint removal by the Goodman et al. (2008) method.

Another method for quantifying the effect of sunglint is to look at the correlation between spectral information and the *in situ* concentration of optically active substances. Empirical relationships are often used as a basis to produce algorithms to estimate the water OAS from remote sensing imagery. Figure 4 shows the distribution of correlation coefficients between various OAS and each spectral band, before and after sunglint removal. It is noticeable that sunglint can obscure the relationship between OAS concentration and spectral information. Once these effects are minimized, correlation coefficients are clearly improved. Nonetheless, there are limited studies comparing the effects of sunglint on estimating water optical properties. In terms of the impact on estimating water depth, Goodman et al. (2008) compared depths derived from processed data to bathymetry derived from Light Detection And Ranging (LiDAR) sensors, under sunglint conditions and after the application of two different deglint procedures (the method proposed by the authors and the method by Hochberg et al., 2003). Goodman et al. method performed better, allowing for correlation coefficients of 0.79 to 0.91, while the method of Hochberg et al. (2003) resulted in correlations of 0.25 to 0.78, and data with no sunglint correction had correlation coefficients of 0.13 to 0.89.

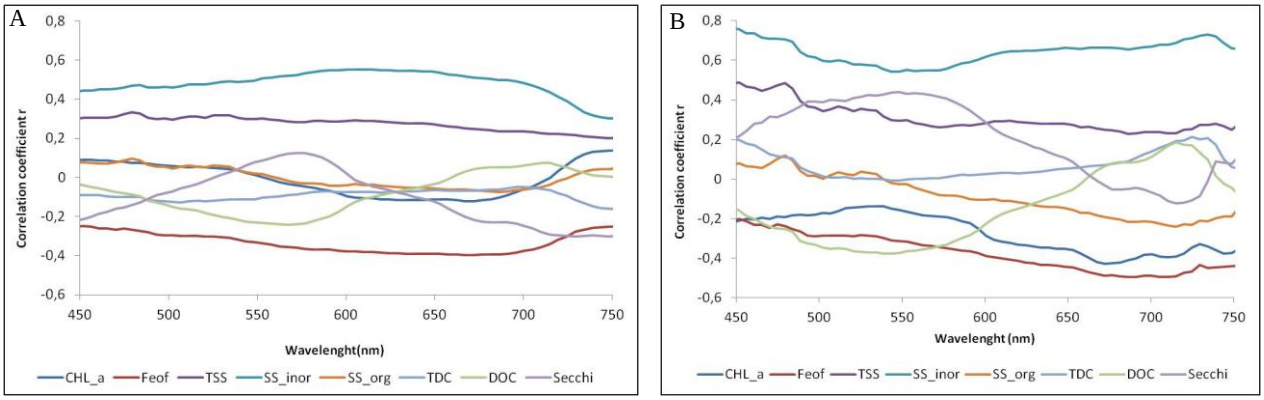


Figure 4. Correlations coefficients between OAS concentration and the image spectral profile corresponding to each water sample station, before (A) and after (B) sunglint removal procedures. CHL_a: chlorophyll-a; Feof: pheophytin; TSS: total suspended solids; SS_inor: inorganic suspended solids; SS_org: organic suspended solids; TDC: total dissolved carbon; DOC: dissolved organic carbon; Secchi: Secchi depth.

4. Conclusions

We have shown that sunglint affects not only the visual aspects of the image, but the magnitude of the spectra, which can lead to errors in the application of classical hyperspectral analysis techniques. The algorithm proposed by Goodman et al. (2008) produced good results when applied to airborne hyperspectral imagery, allowing better visual interpretation of the scenes and improving the correlation coefficients between the concentration of OAS and the spectral information. Sunglint effects had strong spatial variation, which required individual calculations and correction for each image pixel, depending on water roughness. The dynamic approach taken by the Goodman et al. (2008) method allowed for independent corrections on each pixel, and provided a viable solution to mitigate sunglint effects in hyperspectral images of optically complex waters.

Acknowledgments

The authors thank CAPES fellowship supporting Ms. Streher, obtained through the Remote Sensing Graduate Program at INPE, where this research took place. The authors also thank FAPESP for financing the images acquisition through the BIOEN program (08/56252-0) and for the financial support for Dr. Silva (2010/11269-2), FotoTerra for providing the images and Jürgen Langenwalter for the help in interpreting image metadata parameters.

References

Bertels, L.; Vanderstraete, T.; van Coillie, S.; Knaeps, E.; Sterckx, S.; Goossens, R.; Deronde, B. Mapping of Coral Reefs Using Hyperspectral CASI Data; a Case Study: Fordata, Tanimbar, Indonesial. **International Journal of Remote Sensing**., *29*, 2359-2391, 2008.

Casal G., Kutser T., Domingues-Gomez J. A., Sanches-Carnero N. and Freire J**.**, Mapping benthic macroalgal communities in the coastal zone using CHRIS-PROBA mode 2 images. **Estuarine Coastal Shelf Science**. 94, 281–90, 2011.

Dekker, A. G.; Brando, V. E.; Anstee, J. M.; Pinnel, N.; Kutser, T.; Hogenboom, H. J.; Asterkamp, R.; Peters, S. W. M.; C. Olbert, R. J. VOS.; Malthus, T. J. **Imaging spectrometry of water, Imaging Spectrometry: Basic principles and prospective applications**, Dordrecht: Kluwer Academic Publishers, 2001, pp. 307-359.

Ferreira, R. D.; Arnessen, A. S.; Barbosa, C. C. F.; Novo, E. M. L. M. Avaliação do sensor hiperespectral SpecTIR na discriminação de diferentes concentrações de clorofila-*a* no Reservatório de Ibitinga-SP. In: Simpósio Brasileiro de Sensoriamento Remoto. **Anais...** Curitiba, 2011.

Goodman, J.A.; Lee, Z.; Ustin, S.L. Influence of Atmospheric and Sea-Surface Corrections on Retrieval of Bottom Depth and Reflectance Using a Semi-Analytical Model: A Case Study in Kaneohe Bay, Hawaii. **Applied Optics.**, *47*, F1-F11, 2008.

Hedley, J.; Harborne, A.; Mumby, P. Simple and Robust Removal of Sun Glint for Mapping Shallow-Water Benthos. **Int. J. Remote Sens.**, *26*, 2107-2112, 2005.

Hochberg, E.; Andrefouet, S.; Tyler, M. Sea Surface Correction of High Spatial Resolution Ikonos Images to Improve Bottom Mapping in Near-Shore Environments**. IEEE Transactions Geosciences of Remote Sensing**., *41*, 1724-1729, 2003.

Kay, S., Hedley, J.D., Lavender, S.. Sun glint correction of high and low spatial resolution images of aquatic scenes: a review of methods for visible and nearinfrared wavelengths. **Remote Sensing,** v. 1, 697e730, 2009.

Kutser, T.; Vahtmäe, E.; Praks, J.A. Sun Glint Correction Method for Hyperspectral Imagery Containing Areas with Non-Negligible Water Leaving NIR Signal. **Remote Sensing of Environment,**. *113*, 2267-2274, 2009.

Lee Z., Carder, K. Mobley, C. D., Steward, R. and Patch J.. Hyperspectral remote sensing for shallow waters: 2. Deriving bottom depths and water properties by optimization. **Applied Optics**. **38,** 3831-3843,1999.

Lee, K. R.; Olsen R. C. and Kruse Fred A. Using multi-angle WorldView-2 imagery to determine ocean depth near the island of Oahu, Hawaii, , Algorithms and Technologies for Multispectral, Hyperspectral, and Ultraspectral Imagery XVIII… ***Proc. SPIE* 8390**, 2012 http://dx.doi.org/10.1117/12.918716 < Accessed in: 16 nov. 2012>

Lyzenga, D.; Malinas, N.; Tanis, F. Multispectral Bathymetry Using a Simple Physically Based Algorithm. **IEEE Transactions Geosciences of Remote Sensing**. 44, 2251-2259, 2006.

Metsamaa L, Kutser T, Strömbeck N. Recognising cyanobacterial blooms based on their optical signature: a modelling study. **Boreal Environ Res** 11:493–506. 2006.

Mobley, C.D. **The optical properties of water**. New York: McGraw-Hill Book, 1994, 592p.

Moses, W. J., A.A. Gitelson, R. L. Perk, D. Gurlin, D. C. Rundquist, B. C. Leavitt, T. M. Barrow, AND P. Brakhage. Estimation of chlorophyll-a concentration in turbid productive waters using airborne hyperspectral data, **Water Research**, 46: 993-1004, 2012.

Mustard, J.; Staid, M.; Fripp, W. A Semianalytical Approach to the Calibration of AVIRIS Data to Reflectance Over Water Application in a Temperate Estuary. **Remote Sensing of Environment**, *75*, 335-349,2001.

Naumann, J. C.; Young, D. R.; Anderson, J. E. Spatial variations in salinity stress across a coastal landscape using vegetation indices derived from hyperspectral imagery. **Plant Ecology**, v.202, p. 285-297, 2009.

Nush, E. A. Comparison of different methods for chlorophyll and phaeopigment determination. Stuttgart: **Arch. Hydrobiol**. Beih. n. 14, p. 14-39, 1980.

Pontius, J.; Martin, M.; Plourde, L.; Hallet, R. Ash decline assessment in emerald ash borer-infested regions: A test of tree-level, hyperspectral technologies. **Remote Sensing of Environment**, v. 112, p. 2665-2676, 2008.

Vahtmäe, E., Kutser, T., Martin, G., and Kotta, J., Feasibility of hyperspectral remote sensing for mapping benthic macroalgal cover in turbid coastal waters – a Baltic Sea case study. **Remote Sensing of Environment**, 101: 342-351. 2006.